American Mineralogist, Volume 87, pages 142–153, 2002

Correlations of octahedral cations with OH^-, O^{2-}, Cl^-, and F^- in biotite from volcanic rocks and xenoliths

KEVIN RIGHTER,[1,*] M. DARBY DYAR,[2] JEREMY S. DELANEY,[3] TORSTEN W. VENNEMANN,[4] RICHARD L. HERVIG,[5] AND PENELOPE L. KING[6]

[1]Lunar and Planetary Laboratory, University of Arizona, Tucson, Arizona 85721, U.S.A.
[2]Department of Earth and Environment, Mount Holyoke College, 50 College Street, South Hadley, Massachusetts 01075, U.S.A.
[3]Department of Geological Sciences, Rutgers University, Piscataway, New Jersey 08854, U.S.A.
[4]Institute for Geochemistry, University of Tuebingen, Wilhelmstr. 56, 72074
[5]Center for Solid State Science, P.O. Box 871704, Arizona State University, Tempe, Arizona 85287-1704, U.S.A.
[6]Department of Earth Sciences, University of Western Ontario, London, Ontario N6A 5B7, Canada

ABSTRACT

To understand compositional variation in igneous biotite, full analyses of a suite of biotites of variable composition from volcanic and xenolith parageneses have been completed. Major and minor elements were determined by electron microprobe analysis, water was determined by manometry and SIMS analysis, and Fe^{3+}/Fe^{2+} was determined by microXANES and Mössbauer spectroscopy. Our new data, together with previous biotite analyses (total of 52 analyses), reveal correlations between O^{2-} (2-F-Cl-OH) and the sum of the octahedral cations Al + Ti + Fe^{3+} + Cr. This correlation allows estimation of either OH^- or Fe^{3+}/Fe^{2+} as long as one or the other has been determined. The hydroxyl site in most mantle micas contains at least 1.0 O^{2-} atoms per formula unit (apfu), indicating that the oxy-component cannot be ignored. The large oxy-component in melt inclusion micas from the martian meteorite Chassigny does not necessarily indicate oxidized or hydrous magmatic conditions because dehydrogenation may have occurred and/or because the oxy-component may be stable at low oxygen fugacity. The large variation in Ti, Al, and Fe^{3+} in natural igneous micas is most likely dependent upon bulk compositional differences in each specific system such as variation of a_{TiO_2} and $a_{Al_2O_3}$ in silicate melts.

INTRODUCTION

Biotite occurs in a wide variety of settings in igneous rocks and its compositional variation holds information about the conditions under which these rocks formed. Compositional variation is of four forms—that on the tetrahedral sites (cations such as Si, Al, Fe^{3+}), octahedral sites (Mg, Mn, Fe^{2+}, Fe^{3+}, Ti, Al, Cr), the interlayer sites (K, Na, Ba, □), and the "hydroxyl" site (OH^-, O^{2-}, Cl^-, F^-). Past efforts in understanding compositional variation in biotite have been stymied by a variety of problems. Most octahedral and interlayer site cations are easily measured by electron microprobe techniques, but many studies have excluded analysis of BaO, Cr_2O_3, and/or Na_2O, the sum of which can exceed 3 wt% in some biotites. Similarly, some studies include analyses of H_2O, but exclude F^- and Cl^- (and vice versa), thus allowing uncertainty in the nature of the hydroxyl site occupants. Finally, and perhaps most importantly, FeO and Fe_2O_3 are rarely measured in biotites, yet the equilibrium $2FeO + 1/2\ O_2 = Fe_2O_3$ is a function of water and oxygen fugacity and it is linked to the nature of the occupancy of the hydroxyl site. Although complete chemical characterizations including all these variables (and oxygen) are available for a large suite of metamorphic biotites (Dyar et al. 1991, 1993; Guidotti and Dyar 1991), no similar large data set exists for igneous samples.

To better understand the compositional variation in igneous biotites, we have selected and characterized a suite of biotite samples for complete analysis. In this study, we focus on volcanic localities, because their samples are less likely to have experienced re-equilibration of Fe^{3+}/Fe^{2+} or lost OH^-. New data are presented for 16 samples, which together with published biotite analyses, provide new insight into the composition of both terrestrial and martian biotites.

BACKGROUND

Coupled substitution of different cations between tetrahedral (IV), octahedral (VI), and interlayer (XII) sites in micas is complicated, and has been examined in depth by many investigators (see Guo and Green 1990, and references therein), in part because accurate analyses of most of the major-element constituents in mica are possible with electron microprobe analysis (EMPA). For example, in phlogopite the prevalent substitution mechanisms are:

$^{VI}Ti + {}^{VI}\square = 2^{VI}Mg$,
$^{VI}Ti + 2^{IV}Al = {}^{VI}Mg + 2^{IV}Si$, and
$^{XII}Ba + {}^{XII}\square = 2^{XII}K$,

where $^{y}\square$ denotes a vacancy substitution in a site of specified

* E-mail: righter@lpl.arizona.edu

0003-004X/02/0001–142$05.00

coordination (y). Guo and Green (1990) proposed a combined, coupled substitution:

$$^{XII}Ba + 3^{VI}Ti + 4^{IV}Al + {}^{VI}\square + {}^{XII}\square = 2^{XII}K + 4^{VI}(Mg,Fe) + 4^{IV}Si, \quad (1)$$

to explain compositional trends in biotites. Various biotite components are plotted in Figure 1, with the separate substitutions indicated. Righter and Carmichael (1996) also highlighted these major substitution mechanisms for natural and experimental biotites and metamorphic phlogopites, and proposed that the mechanism $^{VI}Ti + 2^{IV}Al = {}^{VI}Mg + 2^{IV}Si$ occurs at high temperatures and pressures.

However, most previous studies did not determine two of the most highly variable chemical constituents of mica: H and Fe^{3+}. Since the early work of Eugster and Wones (1962) first suggested the relationship between Fe^{3+} and OH^- in micas, numerous workers have looked at the substitutions affecting these two variables. Foster (1964) collected analyses of 247 micas for which both H_2O and Fe_2O_3 had been determined. She observed a relatively low degree of correlation between Fe^{3+} and excess O (i.e., H deficiency), and noted that this relationship could explain the amount of OH^- present in only some of the samples studied. As in later studies (Wones and Eugster 1965; Dodge et al. 1969, Ishihara 1977; Barrière and Cotton 1979; Guidotti and Dyar 1991), she concluded that oxygen fugacity probably plays the dominant role in controlling the amount of Fe^{3+} present in a mica. Other studies (e.g., Czamanske and Wones 1973; Chivas 1981; Haslam 1968; Murakami 1969; Redhammer et al. 1993, 1995) have also shown the effect of changing water fugacity on mica Fe^{3+}. These studies demonstrated that both Fe^{3+} and H contents are extremely variable in response to externally imposed buffers.

Studies of naturally occurring samples also show that changes occur in the major element composition of the micas involved in the Fe^{3+}/H equilibrium. In addition to the octahedral and interlayer cation substitutions, there are those involving oxy and hydroxy components and Ti and R^{3+} (R = Fe, Cr, and Al; e.g., Dymek 1983):

$$Al^{3+} + OH^- = Ti^{4+} + O^{2-} + 1/2H_2 \quad (2)$$

and

$$Fe^{2+} + OH^- = Fe^{3+} + O^{2-} + 1/2H_2 \quad (3)$$

Virgo and Popp (2000) showed experimental evidence that Ti is involved in an oxy-substitution mechanism: $Ti^{4+} + 2O^{2-} = M^{2+} + 2(OH^-)$, where M is an unspecified divalent cation. No single substitution mechanism accounts for the variation observed in the analyses of natural biotites, but it is likely that some combination of these substitutions will provide a satisfactory explanation. For instance, it has recently been shown that Fe^{3+} in Ti-rich calcic amphiboles can be calculated as a function of OH^-, Ti, and ^{VI}Al content (King et al. 1999). Because many of the kinds of substitutions relevant to amphibole chemistry are also relevant to biotites, we have examined similar combined substitutions here.

In short, the substitutions that involve (in particular) Fe^{3+} and H in micas are complex and may be intimately related to crystal chemistry and coupled substitutions with other major elements. In any given sample, there is a characteristic $Fe^{3+}/\Sigma Fe$ and OH^-/O^{2-} ratio that reflects the competing effects of externally imposed oxygen and hydrogen fugacity and internal, steric constraints within the mica structure. For this reason, it is always necessary to quantify these variables. Thus in this work, we consider the complete chemical composition of analyzed micas, to develop expressions as a function of major-element compositions that will allow estimation of either Fe^{3+} or H when one or the other has been analyzed.

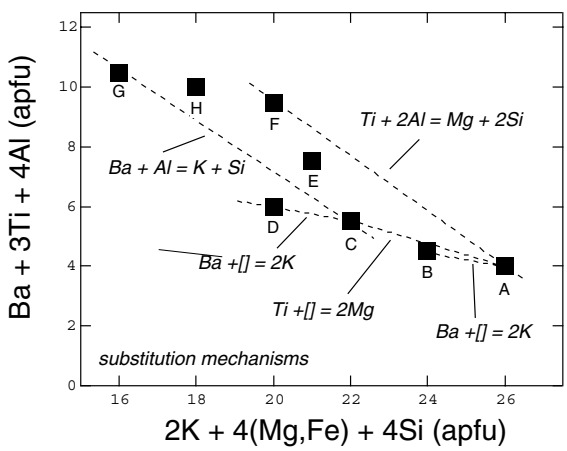

FIGURE 1. Plot of biotite cations, based on the combined substitution mechanism of Guo and Green (1990). Hypothetical components are plotted to illustrate individual substitution mechanisms. The component formulae are as follows: **A** = $KMg_3AlSi_3O_{10}(OH)_2$, **B** = $\square^{XII}_{0.5}Ba_{0.5}Mg_3AlSi_3O_{10}(OH)_2$, **C** = $KMg_2\square^{VI}_{0.5}Ti_{0.5}AlSi_3O_{10}(OH)_2$, **D** = $\square^{XII}_{0.5}Ba_{0.5}Mg_2\square^{VI}_{0.5}Ti_{0.5}AlSi_3O_{10}(OH)_2$, **E** = $\square^{XII}_{0.5}K_{0.5}Mg_{2.5}Ti_{0.5}Al_{1.5}Si_{2.5}O_{10}(OH)_2$, **F** = $KMg_{2.5}Ti_{0.5}Al_2Si_2O_{10}(OH)_2$, **G** = $BaMg_2\square^{VI}_{0.5}Ti_{0.5}Al_2Si_2O_{10}(OH)_2$, **H** = $\square^{XII}_{0.5}Ba_{0.5}Mg_{2.5}Ti_{0.5}Al_2Si_2O_{10}(OH)_2$.

METHODS

Sample selection

For this study, we sought to collect all known published analyses of volcanic biotites for which complete chemical analyses were available. To supplement this data set, which is largely based on wet-chemical analyses, we obtained and analyzed 16 additional samples. Localities and background information for all samples studied are listed in Table 1.

Micro-XANES

Because sample sizes were too small to allow for conventional bulk analysis (wet chemical and Mössbauer) of Fe^{3+}/Fe^{2+} in our biotites, the synchrotron micro-XANES (SmX) method was used (Delaney et al. 1998). X-ray absorption near edge structure (XANES) measurements were made at the synchrotron X-ray microprobe (beamline X26A at the National Synchrotron Light Source of Brookhaven National Laboratory, New York). The structure of the Fe*K*-absorption edge was scanned in the near edge region. Incident beam energies from 50 eV below the main absorption edge energy (7111 eV for Fe) to about 60 eV above the main edge were used. The beam was located by use of an oriented razor blade edge, so beam position could be constrained to within <5–15 μm. Using mutually

TABLE 1. Samples included in this study

Sample ID	Locality	Original reference
	This study (16 new analyses)	
Silver Crater	Silver Crater Mine, Bancroft, Ontario	Sabina (1986)
Mascota	minette, Mascota Volcanic Field Mexico	Carmichael et al. (1996)
San Carlos	megacryst, San Carlos, Arizona	Righter and Carmichael (1993)
Black Canyon	vein, Black Canyon Dike near Hoover Dam	Nielsen and Nakata (1994)
FCT-3	Fish Canyon Tuff	Dan Lux, personal communication
RC-8	Miko Tuff	Dan Lux, personal communication
SLH-2	San Luis Hill, Colorado	none
AMO-16	pumice, Cerro Panizos ignimbrite (Argentina)	Ort (1992)
P87-83	Cerro Panizos ignimbrite (Argentina)	Ort (1992)
BDH-S-9, Kb-9-1, Kb-8-4, Kb-5-10	South African kimberlites	Boettcher and O'Neil (1980)
Sp-55, B-12	biotitite, Rainy Creek Complex, Montana	Boettcher and O'Neil (1980)
Chassigny	martian dunite	Floran et al. (1978); Johnson et al. (1990)
	Literature (36 previously analyzed)	
S23-209, -255, -256, -262, -265, -267, -268, B37-5	East Africa Rift	Feldstein et al. (1996)
Mas-3a, 4, 11, 141	minette, Mascota Volcanic Field Mexico	Feldstein et al. (1996)
LH6	Leucite Hills Volcanic Field, Wyoming	Feldstein et al. (1996)
SN-31, -161	Mono Basin, California	Feldstein et al. (1996)
11	wyomingite, Leucite Hills, Wyoming	Doelter (1917)
15	Fortuna, Murcia	Doelter (1917)
3	fitzroyite, Howe's Hill, W. Australia	Prider (1939)
7	kimberlite, Frank Smith Mine, S. Africa	Williams (1932)
8	kimberlite, Svetlaya dike, Yakutia, USSR	Bobrievich et al. (1964)
9	eclogite, Roberts Victor Mine, S. Africa	Kushiro and Aoki (1968)
OLA9002, 4,12,15,20,23,37,47	Volcan Ollague, Bolivia/Chile	Feeley and Sharp (1996)
BD1150	garnet lherzolite, South Africa kimberlite	Carswell (1975)
Kb-9-1	garnet harzburgite, Bultfontein, S. Africa	Boettcher and O'Neil (1980)
Sp-55, B-12	biotitite, Rainy Creek Complex, Montana	Boettcher and O'Neil (1980)
188/6	nepheline hawaiite dike, W. Texas	Boettcher and O'Neil (1980)
PFIN	phlogopite, Finero	Schmidt et al. (1999)
OKJ	Okenyenya complex, Namibia	Lanyon and LeRoux (1995)

orthogonal Kirkpatrick-Baez mirrors, the beam was focused to a 10×15 μm size. The X-ray sampling depth is probably large but more than 90% of the signal comes from the top 10 μm of the sample. Grains were carefully hand picked from the rocks and all grinding was done under acetone to avoid oxidation from the heat of grinding. Polished grains of the samples were mounted in epoxy on 25 mm lucite disks (standard electron microprobe mounts). The incident beam energy was controlled by a Si(111) channel cut monochromator. The incident X-ray energy was incremented by 0.3 eV intervals over the most critical energy range of –10 to +20 eV relative to the main absorption energy. This provides detailed mapping of the relationship between the pre-edge peak and the main absorption edge for comparison with the magnetite standard (see below) for which the pre-edge position is arbitrarily defined as 0.0 eV. Between –50 and –10 eV and above +20 eV, the X-ray energy was incremented by larger intervals to reduce data collection times. Each energy interval was counted between 5 and 20 live seconds (depending on the intensity of the main edge signal) for a total XANES spectrum acquisition time of about 20 to 30 minutes. Counting times were adjusted to obtain at least 10^5 counts per energy step at energies above the absorption edge. For additional details, see Delaney et al. (1996) and Bajt et al. (1994).

The centroid of a strong pre-edge peak in the compound Fe_3O_4 was used as a reference X-ray energy and all spectra have been plotted relative to that energy. The measured Fe$K\alpha$ fluorescence line intensities were normalized to the ion chamber current and corrected for dead-time. A selected region of the spectrum is fitted to a second-order polynomial (background) plus a Gaussian function (peak). The centroid of the peak is reproducible to within 1% if the peak of interest is the highest peak in the chosen part of the spectrum. Errors in the fitted peak positions were obtained from five independent fits.

The SmX technique uses systematic shifts in the FeK-absorption edge (the energy of a pre-edge peak is measured; Fig. 2A) that vary with oxidation state and coordination (bond strength of Fe-O). Calibration is made using the method of Bajt et al. (1994), which uses the pre-edge peak energies from synthetic fayalite (Fe_2SiO_4), natural magnetite (Fe_3O_4) obtained from the National Museum of Natural History (NMNH), and hematite (Fe_2O_3) to derive a calibration line for determining Fe^{3+} content from pre-edge energy. Pre-edge peak position for the spectrum of each unknown mineral is referenced to the pre-edge peak position of the magnetite spectra run before and after it:

$$\Delta\text{Position}^{\text{unknown}} = \text{Position}^{\text{unknown}}_{\text{measured}} - \text{Position}^{\text{magnetite}}_{\text{measured}}. \quad (4)$$

The regression (calibration) line is fit to the Fe^{3+} contents vs. pre-edge peak positions of fayalite, magnetite, and hematite in each session (and is therefore variable). For a recent session at which biotite measurements were made, for example, the equation was of the form:

$$\%Fe^{3+} = 66.84 + 49.33\ \Delta\text{Position}^{\text{unknown}} \quad (5)$$

Although in most cases it is necessary to use mineral-specific calibrations for minerals in which the Fe sites in the unknown are dramatically different from those of the standards (e.g., garnet, feldspar, quartz, and pyroxene), this is not the

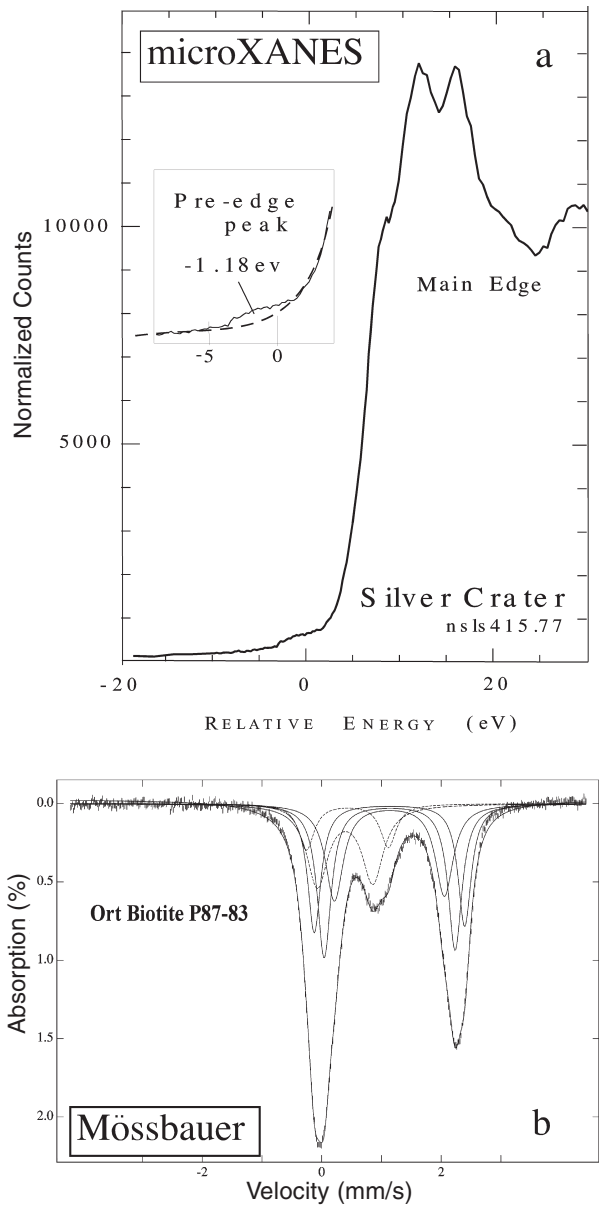

FIGURE 2. (a) Fe*K*-absorption spectrum for biotite from Silver Crater (sample 3, Table 2) showing the main features of the main absorption edge and the pre-edge region used for oxidation state determination. Inset shows the pre-edge region with a spline background fit (dashed line) and the position of the pre-edge centroid after background subtraction indicated. Energy scale is in eV relative to the pre-edge for USNM magnetite standard that provides the primary calibration of ferric/ferrous. Vertical axis is simply normalized intensity. **(b)** Mössbauer spectrum of Ort sample P87-83 (sample 16, Table 2). Spectrum was fit with quadrupole splitting distributions (QSD), two for Fe^{3+} (dashed curves) and three for Fe^{2+} (solid curves). Lorentzian line heights are constrained to be equal, but δ_0, δ_1, Δ, and Δ_0 were allowed to vary (c.f. Rancourt 1994a,b; Rancourt et al. 1994; Rancourt and Ping 1991).

case for biotites as discussed in Dyar (2001). Use of the Bajt et al. (1994) calibration line for biotites yields results that are in good agreement with independent analyses by Mössbauer (Fig. 3); accordingly, their method was used for this study. The current calibration does not account for polarization effects that may be important in micas. Work is in progress to develop correction procedures to account for variation in orientation of individual grains; we need note here only that polarization problems are the major analytical source of error in these measurements. Accuracy for values of $Fe^{3+}/\Sigma Fe$ is believed to be ±10–20%.

Mössbauer analyses

Mössbauer analyses were made on five samples in this study for which adequate amounts of pure separate were available (samples 12 to 16; Table 2). Mössbauer mounts were prepared by mixing sucrose with the sample under acetone. Mounts were prepared to satisfy the ideal absorber thickness approximation of Long et al. (1983) based on the biotite compositions, as recommended by Rancourt et al. (1993).

Room-temperature Mössbauer studies to determine Fe^{2+} and Fe^{3+} content were done in the Mineral Spectroscopy Laboratory at West Chester University. A source of 50–20 mCi ^{57}Co in Rh was used on an Austin Science Associates constant acceleration spectrometer. Run times for the individual measurements averaged two to three days per sample. Results were calibrated against an α-Fe foil of 6 μm thickness and 99% pu-

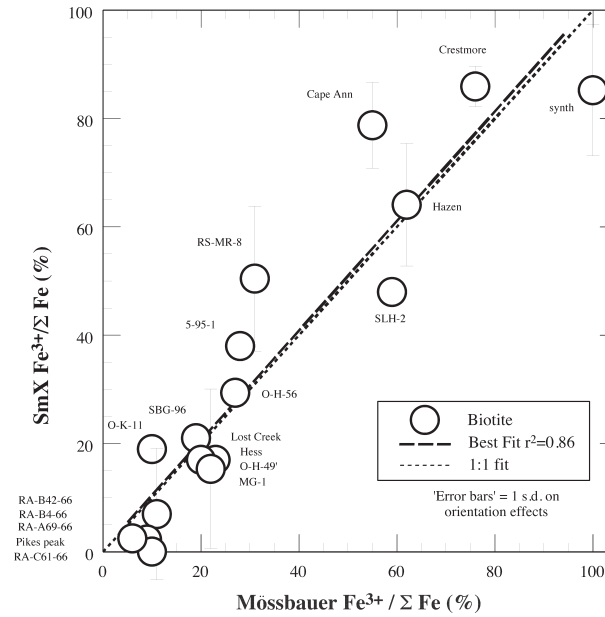

FIGURE 3. Comparison of Mössbauer analyses of $Fe^{3+}/\Sigma Fe$ in separated biotites with synchrotron microXANES (SmX) determinations on single crystals of the same samples. "Error" bars reflect the effect of grain orientation (in a plane parallel to the c-axis) of the biotite on these results and demonstrate X-ray pleochroism in mica. The 1:1 correspondence line and least-squares regression fit are almost indistinguishable. Mössbauer analyses of biotites were collected using the approach of Guidotti and Dyar (1991), and are from Dyar et al. (2001).

TABLE 2. Complete analyses of micas

	1*	2†	3‡	4§	5 B-DH-S-9	6 Sp-55	7 B-12	8 Kb-9-1	9 Kb-8-4	10 Kb-5-10	11 Chass.	12 RC-8	13 SLH-2	14 FCT-3	15 Ort AMO-16	16 Ort P87-83
SiO_2	35.2	39.5	39.2	35.3	38.9	39.4	39.2	43.9	43.6	42.7	39.4	36.15	37.99	36.19	35.43	35.53
TiO_2	7.73	2.64	2.24	7.78	3.53	1.68	1.82	0.73	1.86	0.63	9.30	4.09	4.67	4.51	4.45	4.67
Al_2O_3	15.2	13.88	11.10	15.81	16.72	13.18	13.24	10.44	9.58	9.92	13.09	13.47	12.42	13.52	16.30	15.15
Cr_2O_3	0.00	0.95	n.d.	0.01	0.50	0.30	0.26	0.37	0.19	0.03	–	n.d.	n.d.	n.d.	n.d.	n.d.
Fe_2O_3	3.52	4.24	4.42	1.99	5.99	3.20	5.39	0.66	5.69	6.06	2.63	6.41	8.54	7.46	7.45	8.64
FeO	17.30	1.47	14.43	14.52	0.60	7.80	6.18	2.24	1.45	1.12	9.54	11.71	5.34	9.66	14.62	11.09
MnO	0.21	0.05	0.95	0.11	0.04	0.14	0.13	0.02	0.07	0.04	0.07	0.36	0.10	0.26	0.09	0.07
MgO	9.30	23.11	14.26	11.46	21.23	20.80	20.11	26.56	22.65	25.75	13.70	13.97	17.17	14.45	9.39	11.40
CaO	0.01	0.01	0.00	0.05	0.01	0.00	0.01	0.00	0.01	0.00	0.55	0.03	0.00	0.00	0.00	0.00
BaO	0.37	0.45	0.02	0.65	0.26	0.47	0.49	0.028	0.023	0.15	0.29	0.38	0.30	0.39	0.44	0.39
Na_2O	0.33	0.42	0.44	0.85	1.11	0.14	0.23	0.13	0.56	0.27	0.37	0.37	0.37	0.42	0.25	0.51
K_2O	8.81	9.77	9.43	8.58	8.96	10.19	9.99	10.70	10.62	10.48	7.40	9.33	9.67	9.42	9.54	9.02
H_2O	1.76	2.33	1.54	1.77	2.22	3.20	3.12	3.51	3.19	3.90	0.5	2.49	1.76	1.82	2.15	2.41
F-	0.13	1.23	3.25	0.17	0.36	0.46	0.20	0.29	0.56	0.37	2.08	1.13	2.15	0.59	0.28	0.48
Cl-	0.03	0.03	0.07	0.02	0.02	0.01	0.01	0.03	0.04	0.04	0.4	0.00	0.03	0.00	0.00	0.01
-O=F	0.05	0.52	1.37	0.07	0.15	0.19	0.08	0.12	0.24	0.16	0.88	0.48	0.91	0.25	0.12	0.20
-O=Cl	0.01	0.01	0.02	0.00	0.00	0.00	0.00	0.01	0.01	0.01	0.09	0.00	0.01	0.00	0.00	0.00
X_{Mg}	0.49	0.97	0.64	0.58	0.98	0.83	0.85	0.96	0.97	0.98	0.67	0.68	0.85	0.73	0.53	0.65
Total	99.84	99.55	99.96	99.00	99.97	100.26	99.78	100.83	99.84	101.14	98.35	99.46	99.66	98.45	100.28	99.17
FeO(T)	20.47	5.41	18.40	16.32	5.99	10.67	11.03	4.07	6.57	6.57	11.88	17.48	13.02	16.37	21.33	18.86
Fe	R1	smX	smX	smX	smX	R2	R2	R2	smX	smX	est.	MS	MS	MS	MS	MS
HII	UT#	UT#	UT#	SIMS	R2#	R2#	R2#	SIMS	R2#	R2#	R3	SMU#	SMU#	SMU	SMU	SMU

Notes: FeO and Fe_2O_3 were measured either by Mössbauer spectroscopy (MS), synchrotron microXANES (smX), or were taken from the following references: R1 = Righter and Carmichael (1993); R2 = Boettcher and O'Neil (1980). Values for 11 were estimated as described in the text.

* San Carlos.

† Mascota.

‡ Silver Crater.

§ Black Canyon.

|| H_2O determined by manometry either at Universitat Tuebingen (UT) or Southern Methodist University (SMU), by secondary ion mass spectrometry at Arizona State University (SIMS), or taken from the following references: R2 = Boettcher and O'Neil (1980); R3 = Watson et al. (1994). Microprobe data for samples 15 and 16 is from Ort (1992).

A sample used in the SIMS water calibration (Fig. 4).

rity. Spectra were fit using the program WMOSS from Web Research Co. Both Voigt line shapes in quadrupole pairs and the quadrupole splitting distribution (QSD) model (Rancourt 1994a, 1994b; Rancourt et al. 1994; Rancourt and Ping 1991) were used to fit the spectra (Fig. 2B); results of the two models agreed within the 2% of the total areas, so QSD results were used in Table 2. All Fe was in the octahedral sites, so only Gaussian components corresponding to $^{VI}Fe^{3+}$ and $^{VI}Fe^{2+}$ were needed in the QSD. Differential recoil free-fraction effects were assumed to be negligible (although this may contribute additional error to the results; see Dyar et al. 2001); therefore, the $\%Fe^{3+}$ in the biotites was calculated directly from the proportional peak areas in the spectra. Errors are estimated at ±2% for doublet areas.

Water analyses (manometry and SIMS)

Measurement of water or hydrogen in hydrous minerals can be done using several techniques, including manometry and secondary ion mass spectrometry (SIMS). Three samples (Table 2) were analyzed by T.W.V. using manometric techniques at the University of Tuebingen and the approach outlined by Vennemann and O'Neil (1993). The five samples investigated using Mössbauer spectroscopy in this study (no. 12 to 16; Table 2) were also analyzed for H content by the bulk method using U as a reductant by M.D.D. in the Stable Isotope Laboratory at Southern Methodist University. H contents were determined using a method for volumetric measurement of hydrogen gas generated by reacting water vapor extracted from silicates (Bigeleisen et al. 1952; Holdaway et al. 1986) with either U or Zn. In general, clean mineral separates were degassed under vacuum for at least 8 h at 50 to 150 °C to drive off absorbed atmospheric moisture. Samples were then fused in a silica tube using an oxygen-propane torch or an induction furnace to liberate structural water. Distillation processes involving transfer of evolved gases through a series of liquid nitrogen and alcohol-dry ice slush traps were used to separate water molecules effectively from other condensable and non-condensable gases. Water vapor was then reacted in sealed glass tubes with Zn at 500 °C (Vennemann and O'Neil 1993) or passed over a hot (>750 °C) uranium furnace (Bigeleisen et al.1952; Holdaway et al. 1986) to produce free H_2. The H_2 generated was then expanded on a calibrated inlet of a Finnegan MAT 252 mass spectrometer and the intensity of the mass-2 beam for hydrogen used to determine the yield (Vennemann and O'Neil 1993). Alternatively, a mercury-piston Toepler pump was used to collect hydrogen vapor in a volumetrically calibrated reservoir for yield measurement with a pressure transducer.

Several additional samples from Table 2 were analyzed for water by secondary ion mass spectrometry (SIMS) at Arizona State University (Kb-9-1 and Black Canyon samples; Table 2). SIMS analysis requires a well-characterized set of samples for use as standards. We have assembled a suite of ten biotites for this purpose—five from the study of Boettcher and O'Neil (1980), and five additional from this study, all analyzed for H_2O by manometric techniques (samples Kb-8-4, Kb-5-10, Sp-55, B-DH-S-9, B-12, RC-8, SLH-2, Silver Crater, San Carlos, and Mascota). Full details of the SIMS technique for hydrous minerals are summarized by Ihinger et al. (1994), but the oper-

ating conditions are given here. Ion microprobe analyses of H were obtained with a primary beam of $^{16}O^-$ ions accelerated to 12.5 kV and focussed to a 10–15 μm spot at an intensity of 1.8–1.9 nA. Each analysis consisted of a 7 minute pre-sputter period followed by collection of secondary ion intensities for ^{30}Si and H, at 10 s counting times. Hydrogen count rates were normalized to those for Si, and this ratio was normalized to the SiO_2 content of the mica. The normalized ratio was compared with concentrations of water in standards to derive a calibration curve (Fig. 4). Water contents of the unknown micas were calculated from this curve. Uncertainties in the measured water contents are a result of variation in the H background. The combined analysis of D/H, Fe^{2+}, and Fe^{3+} in micas. This background was minimized and monitored by use of a liquid nitrogen cold trap (following Deloule et al. 1991 and King et al. 1999), and by bracketing unknown analyses with standard analyses during an analytical session. Using these approaches, the error is no greater than ± 0.04 wt% H_2O. In addition, because of the normalization to Si, an additional uncertainty arises from the assumption that the Si^+ intensity is linear with SiO_2 content over the ~20% range (35–44 wt%) in Table 2. However, a study by Steele (1986) suggests that this assumption is warranted, at least over limited ranges in SiO_2 content.

Electron microprobe

Most biotites in this study were analyzed using the Cameca SX50 electron microprobe at the University of Arizona, with a PAP correction procedure. Operating conditions for analysis were 15 kV accelerating voltage, 10 nA sample current, and 10 second counting times. For volatile elements such as Na and K, the count rates decreased with time, and thus these elements were analyzed first. Standards used include a variety of synthetic (diopside, MgF_2) and natural materials (rutile, fayalite, potassium feldspar, sodalite, chromite, barite, rhodonite, albite, and apatite). Samples RC-8, SLH-2, and FCT-3 were analyzed at the University of Houston using a JEOL 8600 Superprobe with Noran (Tracor Northern) automation. Operating conditions were 15 kV accelerating voltage, 20 nA beam current, 30 s count times, and a ~1 μm beam size. Natural and synthetic mineral standards were used and matrix correction was performed using the Noran ZAF routine. Analytical errors on all analyses are 1–2% (relative) for major elements and 5–10% (relative) for minor elements. Multiple analyses were used to check for homogeneity.

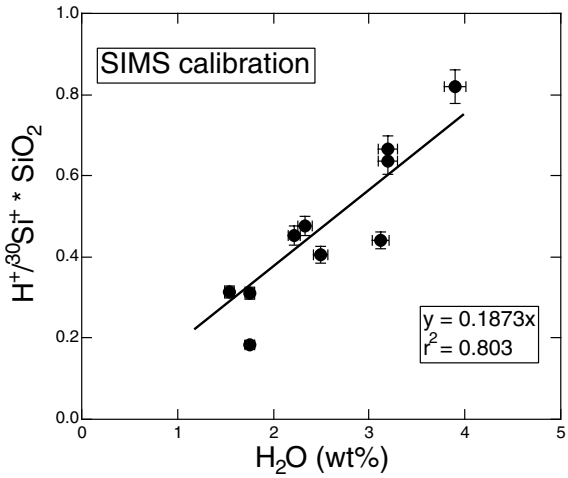

FIGURE 4. Plot of SIMS $H^+/^{30}Si^+ * SiO_2$ vs. H_2O content for a subset of ten samples analyzed for water by manometry (see asterisked samples in Table 2). Data plotted are for samples RC-8, SLH-2, Kb-8-4, Kb-5-10, Sp-55, B-DH-S-9, B-12, Silver Crater, San Carlos, and Mascota (Table 2). SIMS operating conditions are discussed in the text.

Full biotite analyses from this study, including the H_2O, FeO, Fe_2O_3, and bulk composition determinations described in this section, are given in Table 2. Formulae for the fully characterized biotites (Table 3) were calculated on the basis of normalization to 12(O + OH + F + Cl), in accord with the IMA recommendations of Rieder et al. (1998). Based on the 50% rule of solid solution nomenclature (Nickel 1992), sample 1 is annite and samples 2 through 16 are phlogopite.

RESULTS

Using the data set collected for this study, the first objective was to understand the prevalent substitution mechanisms in biotites from volcanic rocks and mantle xenoliths. The coupled substitution proposed by Guo and Green (1990) (Eq. 1, above) was plotted for all available mantle-derived biotites and is illustrated in Figure 5. The data reveal several different substitution mechanisms. Previous work has shown that the mechanism, $^{XII}Ba + {}^{IV}Al = {}^{XII}K + {}^{IV}Si$, may operate at low pressures (Righter and Carmichael 1996), and $^{VI}Ti + 2^{IV}Al = {}^{VI}Mg + 2^{IV}Si$ may operate at higher pressures and temperatures. Two additional mechanisms involve vacancies on the interlayer and octahedral sites, $^{XII}Ba + {}^{XII}\square = 2\ {}^{XII}K$, and $^{VI}Ti + {}^{VI}\square = 2\ {}^{VI}Mg$ (subhorizontal lines in Fig. 5). Some combination of these substitutions can account for compositional variation in mantle micas (Fig. 5).

The second goal was to determine if any relatively simple substitution or coupled substitution could be used to predict Fe^{3+} and H. Any inverse correlation between H^+ and Fe^{3+} would suggest the oxysubstitution mechanism

$$1/2[H_2]_{gas} + Fe^{3+}{}_{mica} \leftrightarrow H^+{}_{mica} + Fe^{2+}{}_{mica} \quad (6)$$

in which hydrogen is incorporated as protons in the crystal structure of mica through a reaction involving oxidation of Fe^{2+} (or consumption of polarons, the excess charge on the Fe^{3+}). Figure 6 shows this relationship for the data set considered here. Although there is a weak inverse relationship, it is clear that the processes controlling Fe^{3+} and H are more complex than Equation 6. In addition, evidence for simple substitutions such as $^{VI}Al^{3+}Fe^{3+}_{-1}$ or $^{XII}(K,Na)Fe^{2+XII}\square_{-1}Fe^{3+}_{-1}$ is not compelling. Similarly, there are no correlations between 2-(OH + F + Cl) and individual cations Fe^{3+}, Ti, and Al (Fig. 7), or the cation pairs (Fe^{3+} + Ti) and (Fe^{3+} + Al) (Fig. 8). Thus, it is necessary to "lump together" all the cation charge variation to develop a predictive equation for Fe^{3+} and H.

CORRELATION BETWEEN O^{2-} AND Σ(Ti, Al, Fe^{3+}, Cr)

There is a good correlation between 2-(OH + F + Cl) and Σ(Ti + Al + Cr + Fe^{3+}) for 52 full biotite analyses (Fig. 9). To

TABLE 3. Formulae for micas (calculated on the basis of normalization to 12 = O + OH + F + Cl)

	1*	2†	3‡	4§	5 B-DH-S-9	6 Sp-55	7 B-12	8 Kb-9-1	9 Kb-8-4	10 Kb-5-10	11 Chassigny	12 RC-8	13 SLH-2	14 FCT-3	15 Ort AMO-16	16 Ort P87-83
Si	2.747	2.860	2.990	2.739	2.794	2.876	2.876	3.086	3.124	3.002	2.979	2.763	2.837	2.804	2.739	2.730
Al	1.253	1.140	0.998	1.261	1.206	1.124	1.124	0.865	0.808	0.822	1.021	1.213	1.093	1.196	1.261	1.270
Fe	0.000	0.000	0.112	0.000	0.000	0.000	0.000	0.049	0.068	0.176	0.000	0.024	0.070	0.000	0.000	0.000
Total (T)	4.000	4.000	4.000	4.000	4.000	4.000	4.000	4.000	4.000	4.000	4.000	4.000	4.000	4.000	4.000	4.000
Al	0.143	0.046	0.000	0.184	0.211	0.011	0.021	0.000	0.000	0.000	0.145	0.000	0.000	0.038	0.225	0.102
Fe^{2+}	1.128	0.089	0.919	0.941	0.036	0.476	0.379	0.132	0.087	0.066	0.603	0.749	0.333	0.626	0.946	0.713
Fe^{3+}	0.209	0.231	0.254	0.116	0.324	0.176	0.298	0.059	0.239	0.144	0.150	0.345	0.410	0.435	0.434	0.499
Mg	1.081	2.493	1.621	1.330	2.275	2.265	2.200	2.782	2.417	2.697	1.544	1.591	1.911	1.669	1.082	1.306
Ti	0.453	0.144	0.128	0.454	0.191	0.092	0.100	0.039	0.100	0.033	0.529	0.235	0.262	0.263	0.259	0.270
Cr	0.000	0.054	0.000	0.001	0.028	0.017	0.015	0.021	0.011	0.002	0.000	0.000	0.000	0.000	0.000	0.000
Mn	0.014	0.003	0.061	0.007	0.000	0.009	0.008	0.001	0.004	0.002	0.000	0.023	0.006	0.017	0.006	0.005
Total (M)	3.028	3.060	2.983	3.124	3.065	3.046	3.021	3.034	2.858	2.944	2.971	2.943	2.922	3.048	2.952	2.895
K	0.876	0.902	0.917	0.849	0.822	0.949	0.935	0.959	0.970	0.939	0.714	0.910	0.921	0.931	0.941	0.884
Na	0.107	0.059	0.065	0.128	0.155	0.020	0.033	0.017	0.078	0.036	0.054	0.055	0.054	0.063	0.038	0.076
Ca	0.001	0.001	0.000	0.004	0.001	0.000	0.000	0.000	0.000	0.000	0.045	0.003	0.000	0.000	0.000	0.000
Ba	0.000	0.013	0.001	0.020	0.000	0.000	0.000	0.000	0.000	0.000	0.009	0.011	0.009	0.012	0.013	0.012
Total (I)	0.984	0.975	0.983	1.001	0.978	0.969	0.968	0.976	1.048	0.975	0.822	0.979	0.984	1.006	0.992	0.972
F	0.032	0.282	0.784	0.042	0.082	0.106	0.046	0.064	0.127	0.082	0.498	0.273	0.508	0.145	0.069	0.117
Cl	0.004	0.004	0.009	0.003	0.002	0.001	0.001	0.004	0.005	0.005	0.051	0.000	0.004	0.000	0.000	0.001
OH	0.916	1.126	0.784	0.917	1.065	1.561	1.529	1.647	1.525	1.830	0.252	1.271	0.877	0.941	1.110	1.236
Total (A)	0.952	1.412	1.577	0.962	1.149	1.668	1.576	1.715	1.657	1.917	0.801	1.544	1.383	1.086	1.179	1.354
Total	8.964	9.447	9.543	9.087	9.192	9.683	9.565	9.725	9.563	9.836	8.594	9.466	9.289	9.140	9.123	9.221

Notes: T, M, I, and A are abbreviations for tetrahedral cations, octahedral cations, interlayer cations, and anions as recommended by the IMA nomenclature for micas (Rieder et al. 1998).
* San Carlos.
† Mascota.
‡ Silver Crater.
§ Black Canyon.

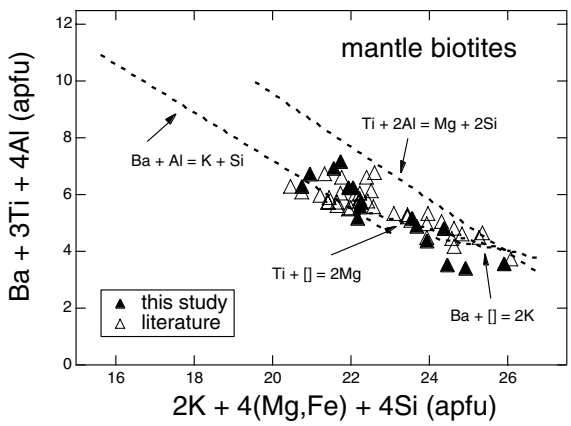

FIGURE 5. Mica analyses from this study (solid triangles), and the literature (open triangles), together with a few of the substitution mechanisms illustrated in Figure 1. Literature data are Aoki (1974), Bobrievich et al. (1964), Boettcher and O'Neil (1980), Dawson et al. (1970), Doelter (1917), Feeley and Sharp (1996), Feldstein et al. (1996), Kushiro and Aoki (1968), Prider (1939), Righter and Carmichael (1993), Williams (1932), and Schmidt et al. (1999).

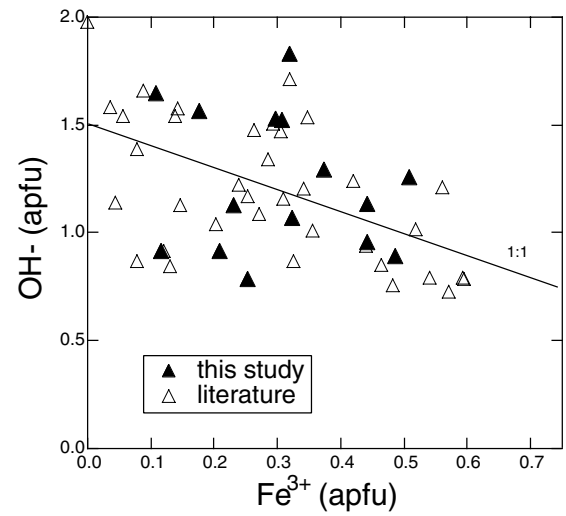

FIGURE 6. The process of dehydrogenation, which involves incorporation of hydrogen as protons in the crystal structure of mica through a reaction that consumes polarons (the excess charge on the Fe^{3+}), leads to a 1:1 inverse relationship between H and Fe^{3+}. Although some of the samples in our data set fall on the 1:1 line, it is clear that the relationship between these variables is generally not so simple. Symbols and data as in Figure 5 (total of 52 analyses).

some extent this correlation is the inevitable result of the normalization procedure, as all of the charge deviation from ideal (i.e., tetravalent charge in the tetrahedral site, divalent in the octahedral sheet, and monovalent charge in the interlayer site) is included. The only deviations from this line result from Ca and vacancy substitution for K and Na. Thus, this correlation represents a combination of cation substitutions such as those outlined in the previous section. For the purposes of this study, the discrimination of specific substitutions is less important than their combined effect as expressed by this correlation line, which allows prediction of any individual analytical variables that might be lacking. Because in many cases investigations cannot determine either $Fe^{3+}/\Sigma Fe$ or total water for particular

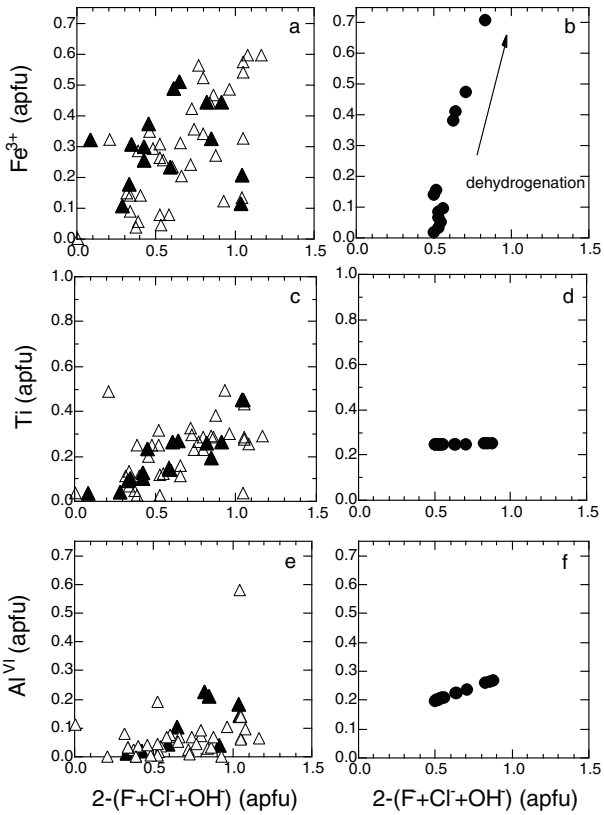

FIGURE 7. Individual cations (Fe^{3+}, Ti, and ^{VI}Al) vs. 2-(F + Cl + OH) for the data shown in Figure 5 (A,C,E), and for the experimentally dehydrated biotites of Virgo and Popp (2000) (B,D,F). Although the latter illustrate systematic behavior for a given bulk biotite composition undergoing dehydrogenation, the larger dataset illustrates that there is not a single substitution mechanism operating in natural biotites.

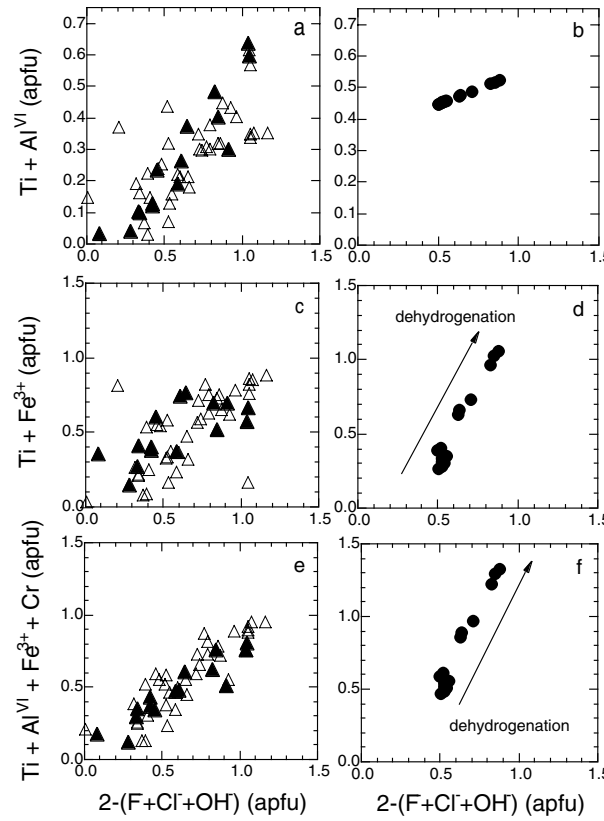

FIGURE 8. Combinations of cations (Ti + ^{VI}Al, Ti + Fe^{3+}, and Fe^{3+} + Cr + Ti + ^{VI}Al) vs. 2-(F + Cl + OH) for the data shown in Figure 6 (A,C,E), and for the experimentally dehydrated biotites of Virgo and Popp (2000) (B,D,F). Again, the latter illustrate systematic behavior for a given biotite bulk composition undergoing dehydrogenation. The combinations of Ti + ^{VI}Al and Ti + Fe^{3+} (A–D) show that even these substitutions do not characterize the compositional variation completely. The combined cations, Fe^{3+} + Cr + Ti + ^{VI}Al, yield the best correlation (E,F) and demonstrate that the variation in oxy-component in these natural micas is accounted for best by a combined substitution mechanism.

samples, this correlation is especially useful, as it allows estimation of either $Fe^{3+}/\Sigma Fe$ or total water if one or the other has not been measured directly. We will discuss below three different applications of this correlation to natural biotites.

DISCUSSION

Dehydrogenation

Before proceeding to natural suites, it is necessary to discuss how dehydrogenation can alter the original composition of biotites (or amphibole; e.g., King et al. 1999; Dyar et al. 1993). The experimental work of Virgo and Popp (2000) can be used to illustrate how biotite composition can change. The correlation of 2-(OH + F + Cl) and Σ(Ti + Al + Cr + Fe^{3+}) observed in the suite of 52 analyses is also mimicked in the experimental samples of Virgo and Popp (2000). A biotite undergoing dehydrogenation will not change in Ti, Cr, or Al content, but the effect of producing Fe^{3+} while losing OH is to drive the composition toward oxy- and Fe^{3+}-rich end-members (Fig. 8). Knowledge of dehydrogenation history of a given sample is thus important to gain a full understanding of the compositional characteristics, as will be evident below.

Mantle biotite

Our compilation of biotite data from mantle samples (xenoliths, kimberlites, megacrysts) reveals a restricted range of Ti + Al + Cr + Fe^{3+}. Given the correlation in Figure 9a, this result implies a large oxy-component for these micas (Fig. 9b). The large oxy-component could be a primary feature of the mantle micas, or it may be due to dehydrogenation either during transport or later cooling. These possibilities are discussed further below.

Although biotite with a large oxy-component might indicate formation under oxidized conditions, it is known that many of these xenoliths equilibrated at reducing conditions, such as FMQ-3 to FMQ + 1 (e.g., Mattioli et al. 1989; O'Neill and Wall 1987; Wood 1990; FMQ = fayalite-magnetite-quartz oxygen buffer). To explore further the relationship between oxygen fugacity and the oxy-component in our micas, we have plotted previously published data from a suite of spinel peridotites that contain either amphibole or biotite and that also

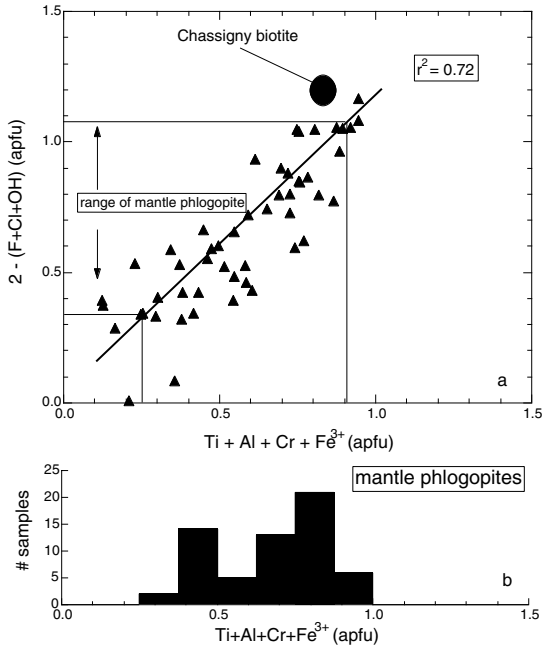

FIGURE 9. (a) Fe + Cr + Ti + Al vs. (2-OH-F-Cl) or O; same data as Figure 6–8. Chassigny biotite is also shown, as is the range of mantle biotite compositions from Figure 9b. **(b)** Histogram of mantle biotite compositions: taken from Matson et al. (1986), Smith et al. (1978), Dawson and Smith (1977), Aoki (1975), Delaney et al. (1980), Jones et al. (1982), Jones and Smith (1984), Lloyd and Bailey (1974), Griffin et al. (1984), Frey and Green (1974), Francis (1976), Nickel and Green (1984), Sen (1988), Bonatti et al. (1986), Ernst (1978), Canil and Scarfe (1989), Wagner et al. (1996).

have spinels that have been analyzed for Fe^{2+}/Fe^{3+}. Oxygen fugacities for these samples have thus been calculated based on spinel-olivine-orthopyroxene equilibria (Mattioli et al. 1989), and biotite analyses are taken from the literature (Fig. 10). There is a distinct negative correlation between (Ti + Al + Cr + Fe^{3+}) in mica and ΔFMQ, indicating that the oxy-component might be stable at more reduced conditions (and assuming equilibrium between mica and the other phases). If this is the case, then perhaps the Fe^{3+} or H contents of the mica are responding to crystal-chemical constraints (such as accommodation of the misfit between tetrahedral and octahedral sheets) rather than fugacity constraints (Redhammer et al. 1993). These results may indicate that the oxy-component can be stable under a broad range of oxygen fugacities, including reducing conditions. In some cases the oxy-biotite component is the dominant one in mantle micas (compared to the fluor, chlor, or hydroxy components) and thus a thorough understanding of the stability fields of mica oxy-end-members is needed to unravel the role of "hydrous" phases in Earth's mantle.

Another way of producing biotite with a large oxy-component is through dehydrogenation (Dyar et al. 2000). Because the variation in 2-(OH + F + Cl) and Σ(Ti + Al + Cr + Fe^{3+}) during dehydration mimics the trend in natural biotites, it is difficult to use bulk compositional data to evaluate dehydrogenation in a given biotite sample or suite of samples. However, D/H ratios may provide useful information as they have for amphiboles (e.g., Deloule et al. 1991). For example, variations of Fe^{3+} and D/H are observed in cores and rims of mantle amphiboles. In some amphiboles, high-Fe^{3+} regions are associated with low δD values, indicating dehydrogenation (Dyar et al. 2000). In other samples, low-Fe^{3+} regions are associated with high δD values, indicating hydrogenation (Dyar et al. 2000). There are currently insufficient δD data for mantle micas to evaluate dehydrogenation on this basis, but this should be a focus of future efforts.

Martian biotite

Knowledge of oxygen fugacity in the martian mantle is important for understanding mantle melting, magma evolution, and core formation on Mars. Oxygen fugacity estimates for the martian mantle generally range from reduced (e.g., Ghosal et al. 1998) to oxidized (McCoy and Lofgren 1996), and any additional constraints that can be provided on this intensive parameter are of great interest.

The Chassigny dunite, proposed to be a piece of Mars, contains many small melt inclusions, one of which contains biotite (e.g., Floran et al. 1978; Johnson et al. 1991). A hydrous mineral such as biotite may indicate hydrous magmatic conditions in the Chassigny parent magma. However, this biotite contains only a small amount of water (~0.5 wt%; Watson et al. 1994), and has a large oxy-component. The biotite has not been analyzed for Fe^{3+}/Fe^{2+} due to its small size, which restricts even microanalytical techniques. However, the $Fe^{3+}/\Sigma Fe$ can be estimated based on analyses of $Fe^{3+}/\Sigma Fe$ in Chassigny clinopyroxene (0.21; Dyar and Delaney 2000), known relations of $Fe^{3+}/\Sigma Fe$ in coexisting clinopyroxene and glass (Righter and

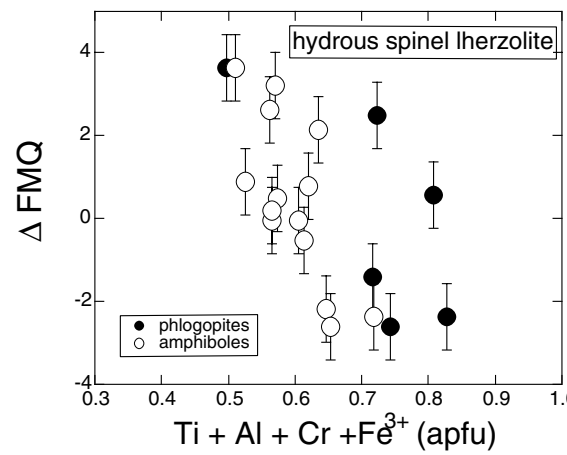

FIGURE 10. Amphibole and biotite (Fe^{3+} + Cr + Ti + Al) vs. ΔFMQ for hydrous spinel peridotites. ΔFMQ was determined in previous studies using olivine–orthopyroxene–spinel oxybarometry (Mattioli et al. 1989). Amphibole and phlogopite compositional data are from studies of Canil et al. (1994), Ionov and Wood (1990), Frey and Green (1974), Press et al. (1986), Frey and Prinz (1978), Ozawa (1988), Takahashi (1980), and Bonatti et al. (1981). ΔFMQ refers to the oxygen fugacity of the sample relative to the fayalite-magnetite-quartz oxygen buffer (O'Neill 1987), according to log f_{O_2} (sample)-log f_{O_2} (FMQ) at an arbitrary temperature of 1200 °C. Values for the log f_{O_2} (sample) were calculated based on spinel–olivine–orthopyroxene equilibria (Mattioli et al. 1989).

Carmichael 1993) and biotite and glass (Righter and Carmichael 1996), giving a value of 0.2 (Table 1). The resulting values for Ti + Al + Cr + Fe^{3+} and (2-OH-F-Cl) for Chassigny biotite (Fig. 9) fall along the trend defined by the other samples from this study and the literature (Fig. 8e). This unusual composition could have formed at oxidized and dry conditions, at reduced and wet conditions, or at reduced and dry conditions.

Although some calculations and measurements have suggested oxidizing conditions in the martian crust, the nearly dry nature of this biotite would require oxygen fugacities as high as the hematite-magnetite buffer or air, well outside the likely range for even the highest f_{O_2} estimates (e.g., McCoy and Lofgren 1996; Righter and Drake 1996). As a result, such an explanation seems unlikely.

If this biotite indeed crystallized from a reduced and hydrous melt, it must have lost its water through a secondary process. Shock processes may cause OH^- loss from hydrous minerals (Minitti and Rutherford 1998), but typically only by a factor of 2 and not enough to account for the severe OH^- depletion in these biotites. Shallow-level magmatic degassing and dehydrogenation is a possibility (Hale et al.1999; Lentz et al. 2000), but if this were the case, the initial biotite composition would not only be OH-rich but would also have low TiO_2 and Al_2O_3 contents (as indicated by the negative correlation between OH and Ti + Al + Cr + Fe^{3+} in Fig. 9), just the opposite of its TiO_2-rich and Al_2O_3-rich composition. Chassigny biotite also does not fall along compositional trends expected for dehydrogenation, such as MgO/(MgO + FeO) vs. Ti + Al + Cr + Fe^{3+} (Fig. 11). As with the terrestrial mantle micas discussed above, stable isotope data may yield information about the extent of dehydrogenation in the Chassigny biotite.

Perhaps the best explanation for the low OH^-, and unusually high TiO_2 (9.30) contents of the Chassigny biotite is that it formed under dry and reduced conditions in the Martian mantle. It is known that the Martian mantle contains much less water than Earth's mantle (50 ppm H_2O, as compared to 480 ppm in the Earth's mantle; Dreibus and Wänke 1989). Dry conditions are also supported by our ion microprobe analysis of the coexisting glass in the Chassigny melt inclusions, which yielded 0.1 wt% H_2O (Righter et al. 1997). In addition, the high oxy-component and the high Ti and Al content may also be a reflection of reducing conditions, as suggested by the correlation in Figure 10. Thus, dry and reducing conditions of formation for the oxy-biotite in Chassigny melt inclusions may be most consistent with the data (FMQ-3; e.g., Righter and Drake 1996). Similar conclusions for the martian mantle were drawn by Mysen et al. (1998) and King et al. (1999) based on high oxy-components of Chassigny kaersutite and other SNC meteorite amphiboles. These new results suggest a reduced mantle, but one that is in general agreement with two-oxide oxy-barometry (e.g., Hale et al. 1999) and pyroxene Fe^{3+}/Fe^{2+} ratios (Ghosal et al. 1998).

Phenocrysts and modeling—importance of the oxy-component

An important observation of this study is the combined correlation of the oxy-component with both Al and Ti contents of the biotites. An understanding of why certain biotites are TiO_2-rich and Al_2O_3-rich would be a great aid in an overall understanding of natural biotite compositional variation. A suggestion

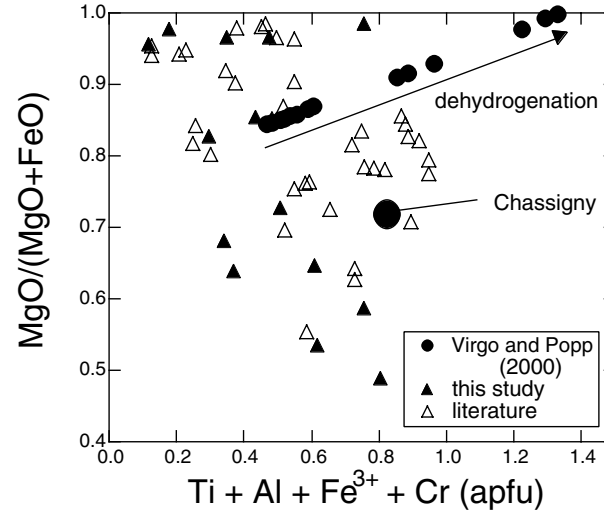

FIGURE 11. A plot of MgO/(MgO + FeO) molar vs. Fe^{3+} + Cr + Ti + ^{VI}Al for biotites from this study, the literature, and those dehydrogenated by Virgo and Popp (2000). Chassigny biotite is shown as a large solid dot. Arrow illustrates change in composition of biotite during dehydrogenation.

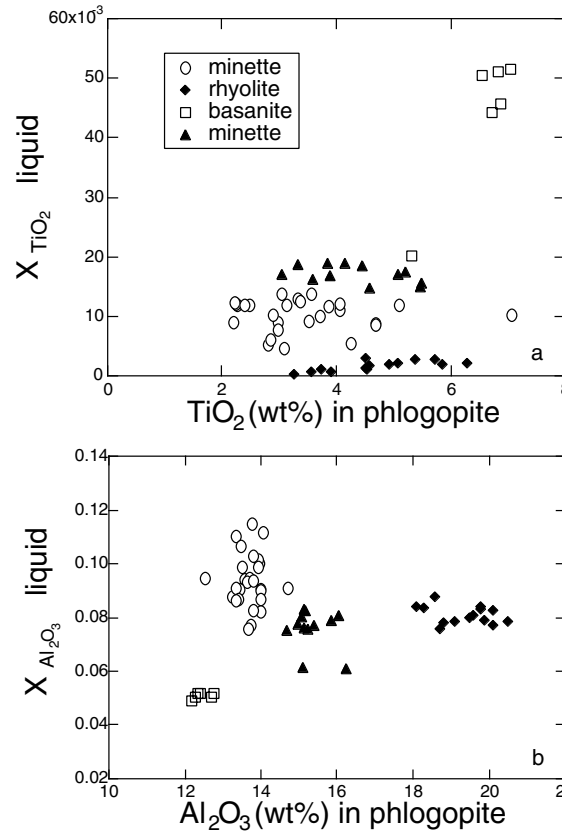

FIGURE 12. (a) Melt TiO_2 and phlogopite TiO_2 for experimental data on rhyolite (Patino-Douce and Beard 1995), minette (Esperanca and Holloway 1987, 1986; Righter and Carmichael 1996), and basanite (Guo and Green 1990) compositions. **(b)** Melt Al_2O_3 and phlogopite Al_2O_3 for same data sets.

by King et al. (1999) that amphibole composition might be dependent upon the activities of Al_2O_3 and TiO_2 in coexisting silicate melts may also be relevant to biotites. Indeed, if one examines experimental biotite-liquid pairs, it is clear that there are strong correlations between biotite and liquid compositions within a given set of experiments (Fig. 12). Note, however, that the correlations between different bulk compositions such as minettes and rhyolites are poor (Fig. 12), indicating that there are other intensive variables involved that can control biotite composition, such as temperature, oxygen fugacity, and bulk composition. Any attempt to model compositional variation in amphiboles and biotites, however, must account for compositional variation in the coexisting melt as well.

ACKNOWLEDGMENTS

Samples for this study were generously provided by Art Montana and N. Cacaglia at UCLA, Michael Ort of Northern Arizona University, Dan Lux of the University of Maine, and Jane Nielson and Howard Wilshire of the USGS-Menlo Park (the latter on loan by Glenn MacPherson and Leslie Hale of the Smithsonian Institution). Bill McDonough provided unpublished microprobe data for Australian amphiboles. Discussions with S. Feldstein and R. Lange, and journal reviews of A. Lalonde, G.F. Redhammer, and M. Fleet were very helpful. This research is supported by NASA grants NAG5-4084, NAG5-9435, NAG5-8820, NAG5-10424, and NSF grants EAR-9806182, EAR-9909587.

REFERENCES CITED

Aoki, K.-I. (1974) Phlogopites and potassic richterites from mica nodules in South African kimberlites. Contributions to Mineralogy and Petrology, 48, 1–7.

———(1975) Origin of phlogopite and potassic richterite-bearing peridotite xenoliths from South Africa. Contributions to Mineralogy and Petrology, 53, 145–156.

Bajt, S., Sutton, S.R., and Delaney, J.S. (1994) X-ray microprobe analysis of iron oxidation states in silicates and oxides using X-ray absorption near edge structure (XANES). Geochimica et Cosmochimica Acta, 58, 5209–5214.

Barrière, M. and Cotton, J. (1979) Biotites and associated minerals as markers of magmatic fractionation and deuteric equilibration in granites. Contributions to Mineralogy and Petrology, 70, 183–192.

Bigeleisen, J., Perlman, M.L., and Prosser, H.C. (1952) Conversion of hydrogenic materials to hydrogen for isotopic analysis. Analytical Chemistry 24, 1356–1357.

Bobrievich, A.P., Lupin, I.P., Kozlov, I.T., Lebedeva, L.I., Pankratov, A.A., Smirnov, G.I., and Kharkov, A.D. (1964) Petrography and mineralogy of the kimberlitic rocks of Yakutia. Nedra, Moscow (in Russian).

Boettcher, A.L. and O'Neil, J.R. (1980) Stable isotope, chemical, and petrographic studies of high-pressure amphiboles and micas: evidence for metasomatism in the mantle source regions of alkali basalts and kimberlites. American Journal of Science, 280A, 694–621.

Bonatti, E., Ottonello, G., and Hamlyn, P.R. (1981) Upper mantle beneath a young oceanic rift: peridotites from the island of Zabargad. Geology, 9, 474–479.

Bonatti, E., Hamlyn, P.R., and Ottonello, G. (1986) Peridotites from the island of Zabargad (St. John), Red Sea: petrology and geochemistry. Journal of Geophysical Research, 91, 599–631.

Canil, D. and Scarfe, C.M. (1989) Origin of phlogopite in mantle xenoliths from Kostal Lake, Wells Gray Park, British Columbia. Journal of Petrology, 30,1159–1179.

Canil, D., O'Neill, H.St.C, Pearson, D.G., Rudnick, R.L., McDonough, W.L., and Carswell, D.A. (1994) Ferric iron in peridotites and mantle oxidation states. Earth and Planetary Science Letters, 123, 205–220.

Carmichael, I.S.E. (1991) The redox state of basic and silicic magmas: a reflection of their source regions? Contributions to Mineralogy and Petrology, 106, 129–141.

Carmichael, I.S.E., Lange, R.A., and Luhr, J.F. (1996) Minettes and related lavas in the Mascota Volcanic Field, Jalisco, Mexico. Contributions to Mineralogy and Petrology, 106, 129–141.

Carswell, D.A. (1975) Primary and secondary phlogopites and clinopyroxenes in garnet lherzolite xenoliths. Physics and Chemistry of the Earth, 9, 417–429.

Chivas, A.R. (1981) Geochemical evidence for magmatic fluids in porphyry copper mineralization. Part I., Mafic silicates from the Koloula igneous complex. Contributions to Mineralogy and Petrology, 78, 389–403.

Czamanske, G.K. and Wones, D.R. (1973) Oxidation during magmatic differentiation, Finnmarka Complex, Oslo Area, Norway: Part 2: The mafic silicates. Journal of Petrology, 14, 349–380.

Dawson, J.B., Powell, D.G., and Reid, A.M. (1970) Ultrabasic xenoliths and lava from the Lashaine Volcano, Northern Tanzania. Journal of Petrology, 11, 519–548.

Dawson, J.B. and Smith, J.V. (1977) The MARID (mica-amphibole-rutile-ilmenite-diopside) suite of xenoliths in kimberlite. Geochimica et Cosmochimica Acta, 41, 309–323.

Delaney, J.S., Smith, J.V., Carswell, D.A., and Dawson, J.B. (1980) Chemistry of micas from kimberlites and xenoliths-II. Primary- and secondary-textured micas from peridotite xenoliths. Geochimica et Cosmochimica Acta, 44, 857–872.

Delaney, J.S., Bajt, S., Sutton, S.R., and Dyar, M.D. (1996) In situ microanalysis of $Fe^{3+}/\Sigma Fe$ in amphibole by x-ray absorption near edge structure (XANES) spectroscopy. Geochemical Society Special Publication 5, 165–171.

Delaney, J.S., Dyar, M.D., Sutton, S.R., and Bajt, S. (1998) Redox ratios with relevant resolution: solving an old problem by using the synchrotron microXANES probe. Geology, 26, 139–142.

Deloule, E., Albarede, F., and Sheppard, S.M.F. (1991) Hydrogen isotope heterogeneities in the mantle from ion probe analysis of amphiboles from ultramafic rocks. Earth and Planetary Science Letters, 105, 543–553.

Dodge, F.C.W., Smith, V.C., and Mays, R.E. (1969) Biotites from granitic rocks of the central Sierra Nevada batholith, California. Journal of Petrology, 10, 250–271.

Doelter, C. (1917) Handbuch der Mineralchemie. Verlag von Theodor Steinkopff, Dresden.

Dreibus, G. and Wänke, H. (1989) Supply and loss of volatile constituents during the accretion of terrestrial planets. In S.K. Atreya, J.B. Pollack, M.S. Matthews, Eds., Origin and Evolution of Planetary and Satellite Atmospheres, p. 268–289. University Arizona Press, Tucson.

Dyar, M.D. (2001) Mössbauer and optical spectroscopy of iron in micas. Proceedings, Micas 2000 Conference, Italian National Academy, Rome, 2000.

Dyar, M.D. and Delaney, J.S. (2000) Correction of the calibration of ferric/ferrous determinations in pyroxene from Martian samples and achondritic meteorites by synchrotron microXANES spectroscopy. Lunar and Planetary Science abstract no. 1981 [CD-ROM].

Dyar, M.D., Colucci, M.T., and Guidotti, C.V. (1991) Forgotten major elements: Hydrogen and oxygen variation in biotite from metapelite. Geology, 19, 1029–1032.

Dyar, M.D., Guidotti, C.V., Holdaway, M.J., and Colucci, M. (1993) Prevalence of oxysubstitution in common rock-forming hydrous silicates. Geochimica et Cosmochimica Acta, 57, 2913–2918.

Dyar, M.D., Delaney, J.S., Kinny, P.D., and Graham, C.M. (2000) Implications of dehydrogenation processes in amphibole for planetary oxygen and hydrogen budgets. Lunar and Planetary Science, abstract no. 1768 [CD-ROM].

Dyar, M.D., Delaney, J. S., and Sutton, S.R. (2001) Fe XANES spectra of iron-rich micas. European Journal of Mineralogy, in press.

Dymek, R.F. (1983) Titanium, aluminum and interlayer cation substitutions in biotite from high-grade gneisses. West Greenland. American Mineralogist, 68, 880–899.

Ernst, W.G. (1978) Petrochemical study of lherzolitic rocks from the Western Alps. Journal of Petrology, 19, 341–392.

Esperanca, S. and Holloway, J.R. (1986) The origin of the high-K latites from Camp Creek, Arizona: constraints from experiments with variable f_{O_2} and aH_2O. Contributions to Mineralogy and Petrology, 93, 504–512.

Esperanca, S. and Holloway, J.R. (1987) On the origin of some mica lamprophyres: experimental evidence from a mafic minette. Contributions to Mineralogy and Petrology, 95, 207–216.

Eugster, H.P. and Wones, D.R. (1962) Stability relations of the ferruginous biotite, annite. Journal of Petrology, 3, 82–125.

Feeley, T.C. and Sharp, Z.D. (1996) Chemical and hydrogen isotope evidence for in situ dehydrogenation of biotite in silicic magma chambers. Geology, 24, 1021–1024.

Feldstein, S.N., Lange, R.A., Vennemann, T., and O'Neil, J.R. (1996) Ferric-ferrous ratios, H_2O contents and D/H ratios of phlogopite and biotite from lavas of different tectonic regimes. Contributions to Mineralogy and Petrology, 126, 51–66.

Floran, R.J., Prinz, M., Hlava, P.F., Keil, K., Nehru, C.E., and Hinthorne, J.R. (1978) The Chassigny meteorite: a cumulate dunite with hydrous amphibole-bearing melt inclusions. Geochimica et Cosmochimica Acta, 42, 1213–1229.

Foster, M.D. (1964) Water content of micas and chlorites. U.S.Geological Survey Professional Papers, F1-F15.

Francis, D.M. (1976) The origin of amphibole in lherzolite xenoliths from Nunivak Island, Alaska. Journal of Petrology, 17, 357–378.

Frey, F.A. and Green, D.H. (1974) The mineralogy, geochemistry and origin of lherzolite inclusions in Victorian basanites. Geochimica et Cosmochimica Acta, 38, 1023–1059.

Frey, F.A. and Prinz, M. (1978) Ultramafic inclusions from San Carlos, Arizona: petrologic and geochemical data bearing on their petrogenesis. Earth and Planetary Science Letters, 38, 129–176.

Ghosal, S., Sack, R.O., Ghiorso, M.S., and Lipschutz, M.E. (1998) Evidence for a reduced, Fe-depleted Martian mantle source region of shergottites. Contributions to Mineralogy and Petrology, 130, 346–357.

Griffin, W.L., Wass, S.Y., and Hollis, J.D. (1984) Ultramafic xenoliths from Bullenmerri and Gnotuk Maars, Victoria, Australia: petrology of a sub-continental crust-mantle transition. Journal of Petrology, 25, 53–87.

Guidotti, C.V. and Dyar, M.D. (1991) Ferric iron in metamorphic biotite and its petrologic and crystallochemical implications. American Mineralogist, 76, 161–175.

Guo, J. and Green, T.H. (1990) Experimental study of Ba partitioning between phlogopite and silicate liquid at upper mantle pressure and temperature. Lithos, 24, 83–95.
Hale, V.P.S., McSween, H.Y., Jr., and McKay, G.A. (1999) Re-evaluation of intercumulus liquid composition and oxidation state for the Shergotty meteorite. Geochimica et Cosmochimica Acta, 63, 1459–1470.
Haslam, H.W. (1968) The crystallization of intermediate and acid magmas at Ben Nevis, Scotland. Journal of Petrology, 9, 84–104.
Holdaway, M.J., Dutrow, B.L., Borthwick, J., Shore, P., Harmon, R.S., and Hinton, R.W. (1986) H content of staurolite as determined by H extraction line and ion microprobe. American Mineralogist, 71, 1135–1141.
Ihinger, P.D., Hervig, R.L., and McMillan, P.F. (1994) Analytical methods for volatiles in glasses. In M.R. Carroll and J.R. Holloway, Eds., Volatiles in Magmas, 30, 67–122. Reviews in Mineralogy, Mineralogical Society of America, Washington, D.C.
Ionov, D.A. and Wood, B.J. (1990) The oxidation state of subcontinental mantle: oxygen thermobarometry of mantle xenoliths from central Asia. Contributions to Mineralogy and Petrology, 111, 179–193.
Ishihara, S. (1977) The magnetite-series and ilmenite-series granitic rocks. Mining Geology, 27, 293–305.
Johnson, M.C., Rutherford, M.J., and Hess, P.C. (1991) Chassigny petrogenesis: Melt compositions, intensive parameters, and water contents of Martian (?) magmas. Geochimica et Cosmochimica Acta, 55, 349–366.
Jones, A.P. and Smith, J.V. (1984) Ion probe analysis of H, Li, B, F and Ba in micas, with additional data for metamorphic amphibole, scapolite and pyroxene. Neues Jahrbuch fuer Mineralogie Monatshefte, 228–240.
Jones, A.P., Smith, J.V., and Dawson, J.B. (1982) Mantle metasomatism in 14 veined peridotites from Bulfontein Mine, South Africa. Journal of Geology, 90, 435–453.
King, P.L., Hervig, R.L., Holloway, J.R., Vennemann, T.W., and Righter, K. (1999) Oxy-substitution in mantle-derived amphibole megacrysts. Geochimica et Cosmochimica Acta, 63, 3635–3651.
Kushiro, I. and Aoki, K. (1968) Origin of some eclogite inclusions in kimberlite. American Mineralogist, 53, 1347–1367.
Lanyon, R. and LeRoux, A.P. (1995) Petrology of the alkaline and ultramafic lamprophyres associated with the Okenyenya igneous complex, northwestern Namibia. South African Journal of Geology, 98, 140–156.
Lentz, R.C.F., Ryan, J.G., Riciputi, L.R., and McSween, H.Y. (2000) Water in the martian mantle: clues from light lithophile elements in martian meteorites. Lunar and Planetary Science XXXI, abstract 1672.
Lloyd, F.E. and Bailey, D.K. (1974) Light element metasomatism of the continental mantle: the evidence and the consequences. Physics and Chemistry of the Earth, 9, 389–416.
Long, G.J., Cranshaw, T.E., and Longworth, G. (1983) The ideal Mössbauer effect absorber thickness. Mössbauer Effect Reference Data Journal, 6, 42–49.
Matson, D.W., Muenow, D.W., and Garcia, M.O. (1986) Volatile contents of phlogopite micas from South African kimberlite. Contributions to Mineralogy and Petrology, 93, 399–408.
Mattioli, G.S., Baker, M.B., Rutter, M.J., and Stolper, E. (1989) Upper mantle oxygen fugacity and its relationship to metasomatism. Journal of Geology, 97, 521–536.
McCoy, T.J. and Lofgren, G. (1996) The crystallization of the Zagami shergottite: a 1 atm experimental study. Lunar and Planetary Science XXVII, 839–840.
Minitti, M.E. and Rutherford, M.J. (1998) Assessment of shock effects on hornblende water contents and isotopic composition. Lunar and Planetary Science XXIX, abstract 1435.
Murakami, N. (1969) Two contrasting trends of evolution of biotite in granitic rocks. Ganseki Kobutsu Kosho Gakkaishi. Journal of the Japanese Association of Mineralogists, Petrologists, and Economic Geologists, 62, 223–247.
Mysen, B.O., Virgo, D., Popp, R.K., and Bertka, C.M. (1998) Amphibole inclusions in SNC meteorites: evidence for a dry martian interior? Lunar and Planetary Science XXIX (abstract).
Nickel, E.H. (1992) Solid solutions in mineral nomenclature. Canadian Mineralogist, 30, 231–234.
Nickel, K.G. and Green, D.H. (1984) The nature of the upper-most mantle beneath Victoria, Australia as deduced from ultramafic xenoliths. In J. Kornprobst, Ed., Kimberlites, II, the mantle and crust-mantle relationships, p. 161–178. Elsevier, Amsterdam.
Nielsen, J.E. and Nakata, J.K. (1994) Mantle Origin and Flow Sorting of Megacryst-Xenolith Inclusions in Mafic Dikes of Black Canyon, Arizona. U.S. Geological Survey Professional Paper 1541, 41 p.
O'Neill, H.St.C. (1987) Quartz-fayalite-iron and quartz-fayalite-magnetite equilibria and the free energy of formation of fayalite (Fe_2SiO_4) and magnetite (Fe_3O_4). American Mineralogist, 72, 67–75.
O'Neill, H.St.C. and Wall, V.J. (1987) The olivine-orthopyroxene-spinel oxygen geobarometer, the nickel precipitation curve, and the oxygen fugacity of the Earth's upper mantle. Journal of Petrology, 28, 1169–1191.
Ozawa, K. (1988) Ultramafic tectonite of the Miyamori ophiolite complex in the Kitakami Mountains, northeast Japan: hydrous upper mantle in an island arc. Contributions to Mineralogy and Petrology, 99, 159–175.
Ort, M.H. (1992) Orbicular volcanic rocks of Cerro Panizos: their origin and implications for orb formation. Geological Society of America Bulletin, 104, 1048–1058.
Patino-Douce, A.E. and Beard, J.S. (1995) Dehydration melting of biotite gneiss and quartz amphibolite from 3 to 15 kbar. Journal of Petrology, 36, 707–738.
Press, S., Witt, G., Seck, H., Ionov, D., and Kovalenko, V. (1986) Spinel peridotite xenoliths from the Tariat depression, Mongolia, I: major element chemistry and mineralogy of a primitive mantle xenolith suite. Geochimica et Cosmochimica Acta, 50, 2587–2599.
Prider, R.T. (1939) Some minerals from the leucite-rich rocks of the West Kimberley area, Western Australia. Mineralogical Magazine, 25, 373–389.
Rancourt, D.G. (1994a) Mössbauer spectroscopy of minerals: I. Inadequacy of Lorentzian-line doublets in fitting spectra arising from quadrupole splitting distributions. Physics and Chemistry of Minerals, 21, 244–248.
———(1994b) Mössbauer spectroscopy of minerals: II. Problem of resolving cis and trans octahedral Fe^{2+} sites. Physics and Chemistry of Minerals, 21, 250–257.
Rancourt, D.G. and Ping, J.Y. (1991) Voigt-based methods for arbitrary-shape static hyperfine parameter distributions in Mössbauer spectroscopy. Nuclear Instruments and Methods, B58, 85–97.
Rancourt, D.G., McDonald, A.M., Lalonde, A.E., and Ping, J.Y. (1993) Mössbauer absorber thickness for accurate site populations in Fe-bearing minerals. American Mineralogist, 78, 1–7.
Rancourt, D.G., Ping, J.Y., and Berman, R.G. (1994) Mössbauer spectroscopy of minerals III. Octahedral-site Fe^{2+} quadrupole splitting distributions in the phlogopite-annite series. Physics and Chemistry of Minerals, 21, 258–267.
Redhammer, G.J., Beran, A., Dachs, E., and Amthauer, G. (1993) Mössbauer and x-ray powder diffraction study of annites synthesized at different oxygen fugacities and crystal chemical implications. Physics and Chemistry of Minerals, 20, 382–394.
Redhammer, G.J., Dachs, E., and Amthauer, G. (1995) Mössbauer spectroscopic and x-ray powder diffraction studies of synthetic mica on the join annite $KFe_3AlSi_3O_{10}(OH)_2$ — phlogopite $KMg_3AlSi_3O_{10}(OH)_2$. Physics and Chemistry of Minerals, 22, 282–294.
Rieder, M., Cavazzini, G., D'Yakonov, Y.S., Frank-Kamenetskii, V.A., Gottardi, G., Guggenheim, S., Koval, P.V., Muller, G., Neiva, A.M.R., Radoslovich, E.W., Robert, J.-L., Sassi, F.P., Takeda, H., Weiss, Z., and Wones, D. (1998) Nomenclature of the micas. Canadian Mineralogist, 36, 905–912.
Righter, K. and Carmichael, I.S.E. (1993) Mega-xenocrysts in alkali olivine basalts: fragments of disrupted mantle assemblages. American Mineralogist, 78, 1230–1245.
———(1996) Phase equilibria of phlogopite lamprophyres from western Mexico: biotite-liquid equilibria and P-T estimates for biotite-bearing igneous rocks. Contributions to Mineralogy and Petrology, 123, 1–21.
Righter, K. and Drake, M.J. (1996) Core formation in Earth's Moon, Mars and Vesta. Icarus 124, 513–529.
Righter, K., Hervig, R.L., and Kring, D.A. (1997) Ion microprobe analyses of SNC meteorite melt inclusions. Lunar and Planetary Science XXVIII, 1181–1182.
Sabina, A.P. (1986) Rocks and minerals for the collector: Bancroft-Parry Sound area and southern Ontario. Geological Survey of Canada, Miscellaneous Report 39, Ottawa.
Schmidt, K.H., Bottazzi, P., Vannucci, R., and Mengel, K. (1999) Trace element partitioning between phlogopite, clinopyroxene and leucite lamproite melt. Earth and Planetary Science Letters, 168, 287–299.
Sen, G. (1988) Petrogenesis of spinel lherzolite and pyroxenite suite xenoliths from the Koolau shield, Oahu, Hawaii: implications for petrology of the post-eruptive lithosphere beneath Oahu. Contributions to Mineralogy and Petrology, 100, 61–91.
Smith, J.V., Brennesholtz, R., and Dawson, J.B. (1978) Chemistry of micas from kimberlites and xenoliths—I. Micaceous kimberlites. Geochimica et Cosmochimica Acta, 42, 959–971.
Steele, I.M. (1986) Ion probe determination of hydrogen in geologic samples. Neues Jahrbuch für Mineralogie, 5, 193–202.
Takahashi, E. (1980) Thermal history of lherzolite xenoliths, I. Petrology of lherzolite xenoliths from the Ichinomegata crater, Oga peninsula, northeast Japan. Geochimica et Cosmochimica Acta, 44, 1643–1658.
Vennemann, T.W. and O'Neil, J.R. (1993) A simple and inexpensive method of hydrogen isotope and water analysis of minerals and rocks based on zinc reagent. Chemical Geology, 103, 227–234.
Virgo, D. and Popp, R.K. (2000) Hydrogen deficiency in mantle-derived phlogopites. American Mineralogist, 85, 753–759.
Wagner, C., Deloule, E., and Mokhtari, A. (1996) Richterite-bearing peridotites and MARID-type inclusions in lavas from North Eastern Morocco: mineralogy and D/H isotopic studies. Contributions to Mineralogy and Petrology, 124, 406–421.
Watson, L.L., Hutcheon, I.D., Epstein, S., and Stolper, E.M. (1994) Water on Mars: Clues from D/H and water contents of hydrous phases in SNC meteorites. Science, 265, 86–90.
Williams, A.F. (1932) The genesis of the diamond. London: Ernest Benn.
Wones, D.R. and Eugster, H.P. (1965) Stability of biotite: experiment, theory, and applications. American Mineralogist, 50, 1228–1272.
Wood, B.J. (1990) Oxygen barometry of spinel peridotites. In D.H. Lindsley, Ed., Oxide Minerals: Petrologic and magnetic significance, 25, 417–432. Reviews in Mineralogy, Mineralogical Society of America, Washington, D.C.

MANUSCRIPT RECEIVED FEBRUARY 6, 2001
MANUSCRIPT ACCEPTED SEPTEMBER 7, 2001
MANUSCRIPT HANDLED BY MICHAEL E. FLEET